

Nonlinear free-surface Rayleigh-Taylor instability

H. J. Kull

*Institut für Angewandte Physik, Technische Hochschule Darmstadt, Hochschulstrasse 2,
D-6100 Darmstadt, Federal Republic of Germany*

(Received 22 July 1985)

The nonlinear evolution of a Rayleigh-Taylor (RT) unstable free surface is studied by three independent approaches. (i) The method of least-squares approximation (LSA) is critically examined and applied to the general RT initial-value problem. It extends previous results of perturbation theories to higher orders and describes the appearance of bubbles and spikes for both single- and multiple-wavelength surface perturbations. Computational limitations, however, are found for the steady-state bubble regime where the number of harmonics becomes exceedingly large. (ii) A mathematically consistent sinusoidal flow model is developed valid for certain nonuniform gravitational accelerations. Its general properties are discussed, including a spike singularity and a unique steady-state bubble shape. As a special case, Layzer's model is obtained and compared with the LSA calculations. (iii) Steady-state bubbles are described more generally in terms of source potentials. A one-parameter family of possible bubble shapes and corresponding gravitational potentials can be derived. It includes the steady-state sinusoidal flow model and yields improved analytic expressions for the constant-acceleration bubble parameters. From this model it is also concluded that flow singularities can limit the general applicability of Fourier analyses to free-boundary flows.

I. INTRODUCTION

In diverse important applications the outcome of hydrodynamic processes depends on the occurrence of Rayleigh-Taylor instabilities. These are well-known interfacial instabilities which develop between superposed fluid layers, when an acceleration is applied towards the denser fluid and similarly under gravity, when a heavy fluid layer is supported by a light one.¹ In particular, RT instabilities have been found of great interest for the study of inertial-confinement fusion.²⁻¹⁰ In standard schemes of fuel compression these represent a major source of asymmetries and thereby limit the attainable fusion energy gain. Occasionally related instabilities have also been discussed in nuclear physics and astrophysics. They provide possible explanations for asymmetric nuclear fission¹¹ as well as for the striking features of elephant-trunk globules in interstellar H II regions.^{12,13} In supernova explosions RT unstable lepton gradients have been predicted, which can potentially cause large scale overturns in the collapsed core.^{14,15} A number of experimental investigations revealed instability growth under various conditions including external,¹⁶⁻¹⁸ ablative,¹⁹ impulsive,²⁰ and magnetic²¹ acceleration.

The nonlinear evolution of the classical RT instability proceeds along three well-known stages of exponential growth, bubble-spike appearance, and steady-state bubble flow.¹⁶ In the following we shall restrict attention to the most severe free-surface instability, which occurs when a fluid layer is supported against gravity by constant gas pressure. Here the bubbles assume the shape of broad columns of gas penetrating the fluid and approaching a constant rise velocity. The spikes consist of narrowing jets of falling fluid separating neighboring bubbles.

The analysis of free-surface motion is conveniently

based on potential theory, where the evolution is governed by a generally nonlinear as well as time-varying boundary condition (Sec. II). A complete mathematical description, however, seems only possible in the linear theory, while the nonlinear evolution requires approximate analyses and numerical evaluations. In previous work various attempts at nonlinear descriptions have been considered, some of which used Fourier analysis,^{17,22-29} conformal mapping methods,³⁰⁻³³ and boundary-integral techniques.³⁴

In this study we shall examine and extend existing methods of Fourier analysis and carefully discuss their applicability to the nonlinear free-surface instability. The Fourier approach is of particular interest, since it allows one to adopt the physical ideas of modes and growth rates developed in the linear theory. The velocity potential can be represented by a superposition of unstable modes which interact through nonlinear mode coupling. This raises questions about the mode spectrum and the growth-rate modification in the nonlinear evolution. But there are also basic questions about the limitations and the general validity of this concept in the nonlinear RT problem. For computational reasons there arise limitations when large numbers of harmonics are required and there are also principle mathematical difficulties, when flow singularities develop so that Fourier series fail to converge. To discuss some of these aspects we compare in the following results obtained by three independent approaches. These are based on the method of least-squares approximation (LSA) and analytic models in terms of sinusoidal and source potentials.

The LSA method has been suggested in the context of RT instability in early works by Hill and Wheeler¹¹ and by Pennington.³⁵ It determines the mode amplitudes by minimizing the mean square error for an expansion of given order. The approach does not presuppose the form

of the time dependence and can also readily be applied to large expansion orders. It therefore extends previous work on second- and third-order perturbation theories.²⁶⁻²⁹ In Sec. III we describe in detail the general procedure and present calculations involving 10-15 modes and 50-100 surface particles. Possibly because of the high numerical resolution, particle redistributions and interpolations have not been required, which greatly simplifies Pennington's original treatment. We also discuss a possible failure of the method which makes it necessary to reconsider the original work. This failure arises when a determinant known as the Gramian approaches zero. In this case the expansion coefficients generally become singular and strongly coupled, although the mean square error can be small. In the present analysis the expansion has been reformulated in terms of orthonormal functions to avoid such artificial failure. Our results, however, still show a rapid increase of higher harmonics when the evolution approaches the steady-flow regime. Therefore these calculations are generally found limited to the initial and transient stages of RT instability.

Further insight in the nonlinear evolution can be gained by the consideration of special flow models. In Sec. IV we analyze fluid motion for a class of sinusoidal flows with time-dependent amplitudes. Single-mode estimates of bubble rise velocities have been given before by Davis and Taylor²² and by Layzer.²³ These nonlinear models describe exactly the particle trajectories in the flow field but satisfy only approximately the dynamical condition of constant surface pressure. Davis and Taylor have studied the steady-state problem with cylindrical symmetry and determined the rise velocity by requiring constant pressure at the bubble vertex and at one further intermediate surface point. Layzer generalized this approach to include the transient evolution and improved the estimate by imposing the constant-pressure condition to the vertex and its immediate neighborhood. This modeling proved rather successful in describing the evolution of bubble amplitudes, but the neglect of harmonics is difficult to justify theoretically.²⁴ We therefore adopt here a different viewpoint which allows us to obtain special exact solutions. For a prescribed class of flows we determine gravitational potentials which consistently satisfy the constant-pressure condition. As a result one obtains possible flows for certain cases of nonuniform acceleration.²⁵ Thus by slightly changing the physical conditions one can avoid major theoretical uncertainties. The model presented illustrates basic features of bubbles and spikes and may be used for testing general computational methods. In particular, it defines precisely the conditions where in the framework of Fourier analysis no harmonics are required in the description of bubble evolution. We also emphasize the important point that the whole class of sinusoidal flows describes asymptotically a unique steady bubble. Its shape is found independent of the initial surface and the transient evolution. Layzer's model is included in the special case where a constant acceleration is prescribed at the bubble maximum. As a result one obtains a special evolution law, which describes the rise velocity in excellent agreement with the least-squares calculations. However, the bubble curvature is found much lower than predicted

for uniform acceleration. In the sinusoidal flow model this is a consequence of an exponentially increasing acceleration along the falling spike.

To obtain more accurate results for uniform acceleration we consider in Sec. V a steady-flow-source model. Here periodic bubble profiles are imitated by the incidence of a uniform stream perpendicular to an infinite row of sources. The source row can be described in complete analogy with vortex rows as commonly studied in the Karman vortex street.³⁶ It is therefore possible to derive explicit analytic expressions for the basic bubble parameters. These are found in excellent quantitative agreement with previous computational results.³²⁻³⁴ The source model also shows principle limitations in the Fourier-series approach. Fourier representations here are only valid in the half-planes above and below the sources and therefore allow no complete description of these flows. Some of the results of Secs. IV and V have already been reported in Refs. 24 and 25. They are presented here in a self-contained form to allow an easy comparison between the different approaches.

In summary, the present discussion of free surface RT instability includes the following results: (i) reformulation of the LSA method to avoid singular expansion coefficients; (ii) LSA calculations of the mode spectrum and of single- and multiple-wavelength surface perturbations; (iii) discussion of computational and mathematical limitations for Fourier analyses; (iv) development of a rigorous sinusoidal flow model extending Layzer's model and comparison with LSA results; (v) derivation of improved analytic expressions for bubble parameters in terms of periodic source potentials.

II. BASIC EQUATIONS

In this section we briefly introduce the basic equations governing the free-surface evolution. We consider an inviscid homogeneous fluid layer of density ρ and pressure p in a gravitational potential $U(y)$. The fluid motion is assumed two-dimensional, irrotational, and incompressible. It is described by the velocity potential $\phi(x,y,t)$ and the corresponding stream function $\psi(x,y,t)$, which are harmonic conjugate functions in the region occupied by the fluid. The velocity components in the x and y directions are defined as the partial derivatives

$$v_x(x,y,t) = \partial_x \phi(x,y,t) = \partial_y \psi(x,y,t), \quad (1)$$

$$v_y(x,y,t) = \partial_y \phi(x,y,t) = -\partial_x \psi(x,y,t),$$

respectively. When the velocity field is given, the evolution of a fluid boundary $y = Z(x,t)$ can be determined from the Cauchy initial-value problem,

$$\begin{aligned} \partial_t Z(x,t) + v_x(x,Z(x,t),t) \partial_x Z(x,t) &= v_y(x,Z(x,t),t), \\ Z(x,0) &= Z_0(x). \end{aligned} \quad (2)$$

This is a single first-order quasilinear partial differential equation for $Z(x,t)$. According to general theory³⁷ its solution can be obtained from a set of characteristic curves $t(p,x_0)$, $x(p,x_0)$, and $y(p,x_0)$ described by

$$\begin{aligned} \frac{dt(p, x_0)}{dp} &= 1, \quad \frac{dx(p, x_0)}{dp} = v_x(x, y, t), \\ \frac{dy(p, x_0)}{dp} &= v_y(x, y, t), \end{aligned} \quad (3)$$

where the initial surface is given parametrically by $t(0, x_0)=0$, $x(0, x_0)=x_0$, and $y(0, x_0)=y_0(x_0)$. The projection of the characteristic curves on the xy plane describes the paths of the surface particles. In the important case where the flow is steady Eq. (2) can easily be integrated. Inserting Eq. (1) into Eq. (2) and requiring $\partial_t Z(x, t) = \partial_t \psi(x, t) = 0$ yields $\psi(x, Z(x)) = \text{const}$. In this case the surface is coincident with a particular streamline.

The evolution of the flow is determined by the condition of constant pressure $p(x, Z, t) = p_0$ on the free surface. This condition is readily expressed using Bernoulli's equation,

$$\partial_t \phi + v^2/2 + p/\rho + U(y) = f(t),$$

where $v^2 = v_x^2 + v_y^2$ and the time function $f(t)$ is fixed by the values of the left-hand side in one particular point of the fluid. We now choose the special gauge of the potential where $f(t) = p_0/\rho$. Then the free-surface boundary condition becomes

$$\partial_t \phi(x, Z, t) + v^2(x, Z, t)/2 + U(Z) = 0. \quad (4)$$

One should, however, notice that with this special gauge the velocity potential generally does not vanish at infinity ($y \rightarrow +\infty$) where the fluid is at rest.

Sometimes it is more convenient to describe the evolution in the coordinate frame rising with the bubbles. The origin then is attached to the bubble vertex $x=0$, $y=a(t)$ moving with the bubble velocity $u = \dot{a}$ in the y direction. In this comoving frame the fluid motion can still be described by a potential; however, the boundary conditions are changed (Appendix A). At infinity, where the fluid is at rest, the boundary condition becomes $v_y(x, +\infty, t) = -u$, and at the free surface,

$$\partial_t \phi(x, Z, t) + v^2(x, Z, t)/2 + U(a+Z) - U(a) + \dot{u}Z = 0. \quad (5)$$

Here a gauge has been used, where $\partial_t \phi(0, 0, t) = 0$, and the bubble acceleration \dot{u} introduces an additional effective body force.

In the following we shall suppose periodicity in x with wave number $k = 2\pi/\lambda$ and express, unless otherwise stated, lengths in units of k^{-1} and times in units of $(gk)^{-1/2}$, where g denotes the unit of gravitational acceleration. Further assuming even symmetry with respect to $x=0$, the Fourier-series representation of the potential assumes the form

$$\phi(x, y, t) = \frac{1}{2} a_0(t, y) + \sum_{m=1}^{\infty} a_m(t, y) \cos(mx). \quad (6)$$

Since ϕ must satisfy the Laplace equation and the boundary condition $v_y(x, +\infty, t) = 0$ the Fourier coefficients $a_m(t, y)$ can be written as

$$a_m(t, y) = \phi_m(t) e^{-my}$$

for $m \geq 0$. The evolution is governed by the time depen-

dence of the amplitudes $\phi_m(t)$. As discussed in the following section this is determined by the free-surface boundary condition (4). We finally note that in the frame comoving with the bubbles the flow may be described by corresponding amplitudes $\phi'_m(t)$. The transformation (A2) of the potentials implies for the amplitudes the transformations

$$\phi'_m(t) = \phi_m(t) e^{-ma}, \quad m \geq 1.$$

III. LEAST-SQUARES APPROXIMATION

To analyze the formation of bubbles and spikes in the nonlinear RT instability we first consider a numerical procedure introduced by Pennington.³⁵ It is based on the method of least squares to approximate the potential by a set of basic harmonic functions and leads to a closed set of ordinary differential equations.

Let us assume that the velocity potential can be represented in the form $\phi = f(x, y, t, c_m(t))$, with time-dependent parameters $c_m(t)$ labeled by the subscript $m = 0, 1, 2, \dots$. Here f is considered as a known function of its arguments. It is harmonic with respect to the spatial coordinates x, y and satisfies at the fixed boundaries the conditions $\partial_x f(x=0) = \partial_x f(x=\pi) = \partial_y f(y=+\infty) = 0$. Specifically, for the Fourier-series representation (6) the function f is given by

$$\begin{aligned} f(x, y, t, c_m(t)) &= \sum_{m=0}^{\infty} c_m(t) f_m(x, y), \\ f_m(x, y) &= e^{-my} \cos(mx). \end{aligned}$$

In this case it depends linearly on the parameters $c_m(t)$ and contains no explicit time dependence. The evolution of the parameters c_m is governed by the free-surface boundary condition. Using a parametric representation of the surface $x = x(x_0, t)$, $y = y(x_0, t)$, Eq. (4) assumes the general form

$$\begin{aligned} \sum_m \dot{c}_m(t) f_m(x(x_0, t), y(x_0, t), c_m, t) \\ = R(x(x_0, t), y(x_0, t), c_m, t) \end{aligned} \quad (7)$$

with $f_m = \partial_{c_m} f$ and $R = -(\partial_t f + v^2/2 + U)$. At a given time the function R depends on x_0 only and the time derivatives \dot{c}_m are the coefficients in a series expansion of R with respect to the set of functions $\{f_m\}$. The coefficients will now be determined by the method of least squares. We define

$$(a, b) = \frac{2}{\pi} \int_0^\pi dx_0 a(x(x_0), y(x_0)) b(x(x_0), y(x_0)),$$

$\|a\| = (a, a)^{1/2}$, for functions $a(x, y)$ and $b(x, y)$ and approximate R by a linear combination of r functions such that the mean square error $\|\sum_{m=0}^{r-1} \dot{c}_m f_m - R\|^2$ becomes least. The minimum is assumed if the coefficients \dot{c}_m obey the r -component vector system,

$$F \cdot \mathbf{x} = \mathbf{R} \quad (8)$$

with the vector and matrix components defined by $x_m = \dot{c}_m$, $R_m = (f_m, R)$, and $F_{mn} = (f_m, f_n)$, respectively.

If the determinant $\Gamma = |F_{mn}|$ does not vanish Eq. (8) together with Eq. (3) determines uniquely the evolution of an approximate solution from the initial conditions. If s is the number of surface particles the system consists of $2s + r$ coupled first-order differential equations.

Let us now consider the failure of the procedure if the determinant approaches zero. This case generally leads to a singular behavior of the expansion coefficients even if the ansatz is an accurate approximation to the solution. To discuss this important point in some detail we note that Γ is known as the Gram determinant of the functions $\{f_m\}$, where here and in the following discussion we always refer to the functional dependence on x_0 . Let λ_i with $i=0, 1, \dots, r-1$ denote the eigenvalues of the symmetrical matrix F and e^i the corresponding eigenvectors normalized by $e^i \cdot e^i = 1$. One can then define a set of mutually orthogonal functions $\{\tilde{f}_i\}$ by observing that

$$\tilde{f}_i = \sum_{m=0}^{r-1} f_m e_m^i, \quad (\tilde{f}_i, \tilde{f}_j) = e^i \cdot F \cdot e^j = \lambda_j \delta_{ij}, \quad (9)$$

where δ_{ij} are the elements of the unit matrix. From Eq. (9) it follows immediately that the Gram determinant $\Gamma = \prod_{i=0}^{r-1} \lambda_i$ is non-negative and can be zero if and only if the functions f_m are linearly dependent. Let us now suppose that Γ approaches zero in the course of time evolution. To obtain the behavior of the coefficients \dot{c}_m in this limit we represent the solution of Eq. (8) as a linear combination of the eigenvectors e^i . If all eigenvalues are nonzero, Eqs. (8) and (9) yield

$$\mathbf{x} = \sum_{i=0}^{r-1} \lambda_i^{-1} (\mathbf{R} \cdot e^i) e^i = \sum_{i=0}^{r-1} \lambda_i^{-1} (\tilde{f}_i, \mathbf{R}) e^i. \quad (10)$$

In the limit $\lambda_j \rightarrow 0$ the projection $(\tilde{f}_j, \mathbf{R})$ generally approaches zero as $\|\tilde{f}_j\| = (\lambda_j)^{1/2}$ and then the solution (10) is seen to become singular as $\lambda_j^{-1/2}$. However, in the approximating series,

$$\sum_{m=0}^{r-1} \dot{c}_m f_m = \sum_{i=0}^{r-1} \frac{(\tilde{f}_i, \mathbf{R}) \tilde{f}_i}{(\tilde{f}_i, \tilde{f}_i)}, \quad (11)$$

the singular coefficient is multiplied by a function of vanishing norm so that the contribution there remains finite and even may be negligibly small.

To avoid the difficulty of singular coefficients in this case we consider an expansion with respect to an orthonormal function system. Suppose the ansatz f has the form of a series with basic functions $f_m(x, y)$. Then it can be rewritten in the form

$$f(x, y, t, c_m) = \sum_m c_m(t) g_m(x, y, t) \quad (12)$$

with an orthonormal set $\{g_m = h_m / \|h_m\|\}$ defined by the Gram-Schmidt orthonormalization procedure where

$$h_m = f_m - \sum_{i=0}^{m-1} (g_i, f_m) g_i.$$

Note that the set $\{g_m\}$ has an explicit time dependence since the inner product is defined on the time-dependent surface. The corresponding time derivative $\partial_t f$ in the function R of Eq. (7), however, can be calculated from

known quantities at a given time as shown in Appendix B. The elements of the Gram matrix now are $(g_m, g_n) = \delta_{mn}$ and therefore Eq. (8) assumes the simpler form

$$\dot{c}_m = (g_m, \mathbf{R}). \quad (13)$$

We emphasize that the derivatives here are independent of each other and of the order r of the expansion. One may therefore conveniently omit linearly dependent terms without changing the remaining derivatives. The coefficients also directly indicate the relevant order of magnitude of the expansion terms.

We now discuss some computational results obtained for a Fourier-series representation of the potential where $f_m(x, y) = \exp(-my) \cos(mx)$. This expansion describes the flow when all singularities of the potential lie in the half-plane below the lowest surface point. It may therefore be valid for a transient phase only. Equations (3) and (13) have been numerically integrated with expansion orders $r=10-15$, particle numbers $s=50-100$, constant acceleration $U(y)=y$, and initial conditions

$$c_m(0) = 0, \quad (14)$$

$$Z_0(x) = A \cos x + B \cos(2x) + C \cos(3x).$$

In the given range the results showed only negligible vari-

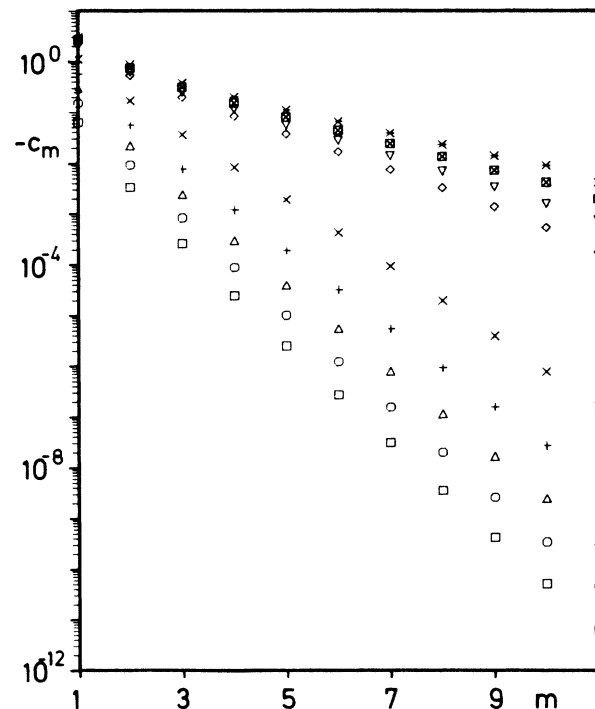


FIG. 1. Evolution of the mode amplitudes in the LSA calculation. The representation shows the coefficients $-c_m$ as defined in Eq. (12) vs mode number m . Initially the fluid is at rest ($c_m=0$) with a sinusoidal surface displacement of amplitude 0.1. The different marker symbols denote the subsequent times $t=0.6, 1.2, 1.8, 2.4, 3.0, 3.6, 3.7, 3.8, 3.9$. Note that the time step has been reduced after $t=3.6$ because of the rapid increase of higher harmonics.

ations with r and s . The numerical analysis has been tested by comparison calculations between the laboratory and bubble coordinate frames which have been found in excellent agreement.

To verify the validity range of the present approximations we first examine the case of a purely sinusoidal initial perturbation where $A=0.1$ and $B=C=0$. Figure 1 shows the mode spectrum given by the amplitudes c_1 up to c_{11} of the series (12) at a sequence of times. The coefficient c_0 describes only the gauge of the potential and therefore has been omitted from the representation. Notice that in an initial stage the flow is well approximated by a few terms of the Fourier series. At time $t=0.6$ the mean error of the approximating series $\|\sum_{m=0}^{11} c_m g_m - R\|/\|R\|$ is found to be of the order 10^{-12} . However, during the time evolution the convergence of the series becomes increasingly worse. At the final time $t=3.9$ the mean error has grown up to the order 10^{-1} and the Fourier ansatz then ceases to be an appropriate representation. We also considered the expansion coefficients obtained from Eq. (8) without the orthonormalization procedure. These have been found to depend strongly on the expansion order and the calculations there failed around the time $t=3.6$ where the matrix became algorithmically singular. Figure 2 shows a sequence of surface profiles at the times indicated in Fig. 1. One can

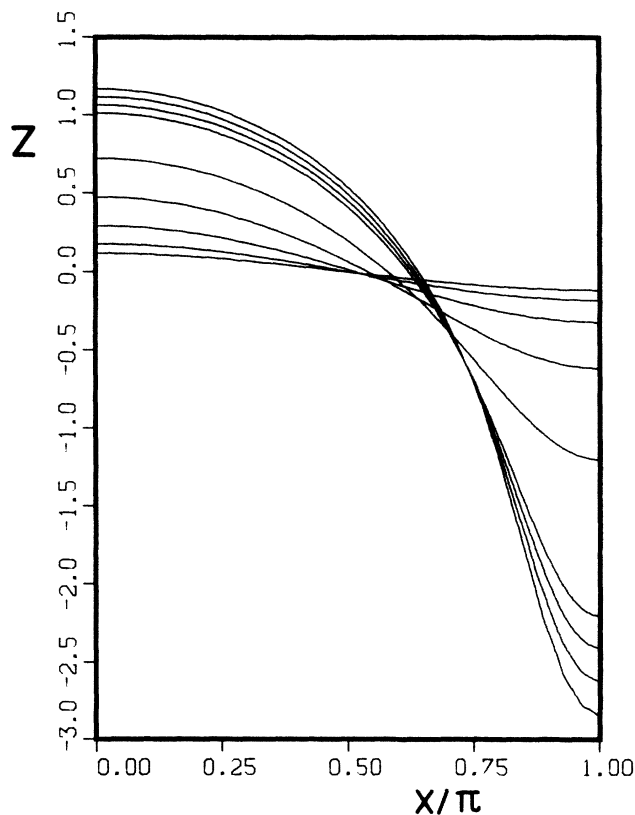


FIG. 2. Surface profiles corresponding to the initial conditions and time steps given in Fig. 1. In the nonlinear evolution the sinusoidal perturbation becomes asymmetric, leading to the characteristic bubble-spike shape.

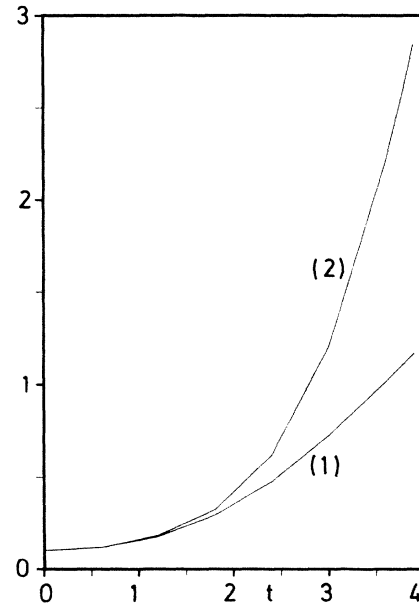


FIG. 3. Evolution of bubble (1) and spike (2) amplitudes.

recognize the formation of a rising gas bubble around $x=0$ and of a falling spike around $x=\pi$. In the present description this is a result of nonlinear mode coupling between the fundamental mode and the first ten harmonics. To study the asymmetrical growth in detail the bubble and spike amplitudes have been represented in Fig. 3. There symmetry deviations already become appreciable for amplitudes larger than about 0.3–0.4. At the final time the total bubble spike separation is about 4, which is somewhat larger than half a wavelength. Let us finally consider some examples of multiple-wavelength perturbations. The evolution can be drastically changed if neighboring modes reach the nonlinear regime simultaneously. The situation is illustrated in Fig. 4 for the fundamental mode with initial amplitude $A=0.1$ and the first harmonic with initial amplitudes $B=\pm 0.01$. Note that the first harmonic reaches large amplitudes during the calculation (a) so that the nonlinear superpositions (b) and (c) yield strongly disturbed profiles. Similar results for the second harmonic with $C=\pm 0.005$ are given in Fig. 5.

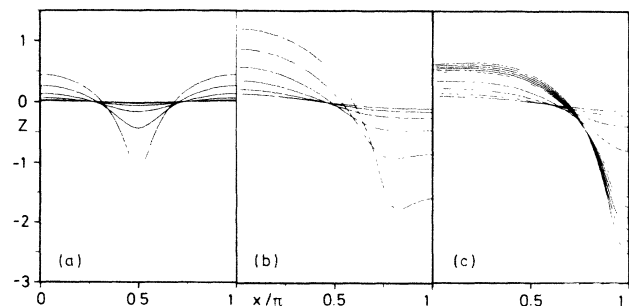


FIG. 4. Multiple-wavelength surface perturbations with initial conditions (a) $A=0.0$, $B=0.1$, (b) $A=0.1$, $B=0.01$, and (c) $A=0.1$, $B=-0.01$. The time step is 0.6 up to $t=3.6$ in (a) and (b), and then 0.1 up to $t=4.0$ in (c).

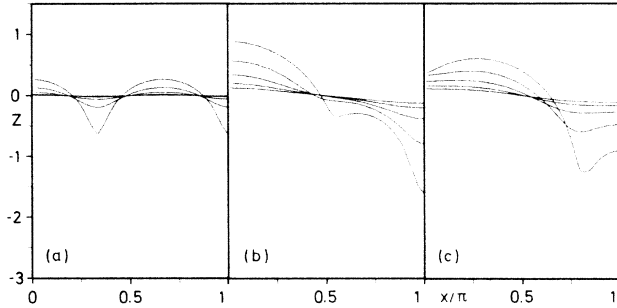


FIG. 5. Multiple-wavelength surface perturbations with initial conditions (a) $A = 0, C = 0.005$, (b) $A = 0.1, C = 0.005$, and (c) $A = 0.1, C = -0.005$. The time step is 0.6 and the final time 3.0.

IV. SINUSOIDAL FLOWS

Least-squares approximation provides a general approach to the classical RT initial-value problem. However, the preceding analysis has shown that an exceedingly large number of expansion terms is required before the final adjustment to a steady state takes place. To obtain better insight into the basic nonlinear features we will now examine some analytic models of bubble formation and bubble motion. We will proceed by first analyzing some fluid motions around bubbles without gravity and then defining gravitational potentials which satisfy the constant-pressure boundary condition at the free surface.

In this section we restrict attention to purely sinusoidal velocity fields. These may be considered as the most simple periodic flows since harmonics and possible singularities there are neglected. The velocity potential and the stream function assume the general form

$$\phi(x, y, t) = \phi_0(t) - A(t)e^{-y} \cos x, \tag{15}$$

$$\psi(x, y, t) = \psi_0(t) - A(t)e^{-y} \sin x.$$

To specify the flow direction we take $A(t) > 0$. Let us first examine the evolution of a fluid boundary. This is most easily done by observing that the streamlines are steady and therefore coincident with the particle trajectories. At each instant of time the streamline through an arbitrary reference point (x_0, y_0) is defined by $\psi(x, y, t) = \psi(x_0, y_0, t)$ yielding

$$y = y_0 + \ln(\sin x / \sin x_0). \tag{16}$$

These streamlines emerge from $y = -\infty$ at $x = 0$, reach a maximum at $x = \pi/2$, and are bent back towards $y = -\infty$ at $x = \pi$ (Fig. 6). The particles at $x = 0$ and π only move vertically. Their trajectories are easily obtained as

$$y(t) = y_0 + \ln \left[1 \pm e^{-y_0} \int_0^t A(t) dt \right], \tag{17}$$

respectively. Denoting $y(x_0 = 0, y_0 = a_0, t) = a(t)$, the horizontal motion of a particle with initial coordinates x_0, y_0 assumes the form

$$x(t) = x_0 + (e^a - e^{a_0})e^{-y_0} \sin x_0. \tag{18}$$

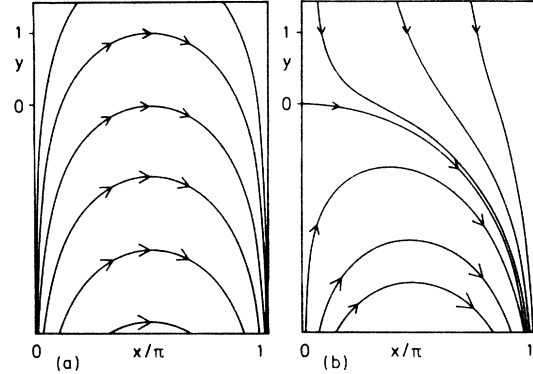


FIG. 6. Streamline patterns for sinusoidal velocity fields. (a) Laboratory frame where the fluid is at rest at $y = +\infty$. (b) Comoving frame with a stagnation point at the origin. The separatrix starting from the stagnation point defines the asymptotic bubble profile.

Equations (16)–(18) give a parametric representation of the evolution of an initial surface $y_0 = y_0(x_0)$. As an example Fig. 7 shows the evolution of a fluid layer $y > 0$ where the initial surface is given by $y_0(x_0) = 0$. We will be interested in the asymptotic surface profile which is approached with increasing amplitudes $a(t)$. According to Eq. (18) surface particles in $0 < x_0 < \pi$ move away from the line $x = 0$. At late times the head of the bubble therefore consists of the particles with initial positions near $x_0 = 0$. Expanding Eq. (18) about $x_0 = 0$ and putting $a_0 = y_0(0)$ yields $x = x_0 e^{a - a_0}$. Then eliminating x_0 from Eq. (16), the asymptotic surface profile is found to be

$$y = a + \ln(\sin x / x). \tag{19}$$

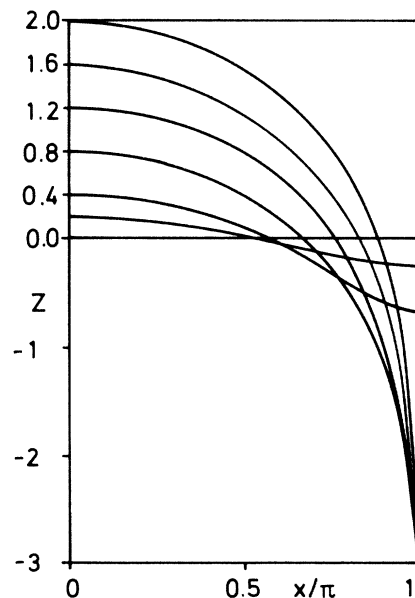


FIG. 7. Surface evolution of the fluid layer $y > 0$ in the sinusoidal flow model.

It describes a bubble of amplitude $a(t)$ at $x=0$ and a jet extending to infinity at $x=\pi$. It is important to note that the bubble shape is independent of the initial profile and the special evolution of $a(t)$. Thus it is a common feature of the whole class of flows described by Eq. (15). Another peculiarity of these flows consists in the fact that the falling jet reaches infinity at a finite bubble amplitude, $a=a_0+\ln\{1+\exp[y_0(\pi)-a_0]\}$. Then fluid is continuously absorbed at infinity which, however, does not violate the flow within a finite region. The analysis is even more straightforward in the comoving bubble coordinate frame. There the flow will be described by

$$\phi = \phi_0 - \dot{a}(y + e^{-y}\cos x), \tag{20}$$

$$\psi = \psi_0 + \dot{a}(x - e^{-y}\sin x),$$

and the streamlines $\psi(x,y,t)=\psi(x_0,y_0,t)$ have the form

$$y = \ln[\sin x / (x - b)], \quad b = x_0 - e^{-y_0}\sin x_0. \tag{21}$$

The asymptotes to the streamlines for $y \rightarrow +\infty$ are given by $x=b$ and the separatrix between streamlines entering at $y = +\infty$ and $-\infty$ is obtained by setting $b=0$. Fluid motion along the separatrix is seen to determine the final bubble shape (Fig. 6).

Having reviewed the fluid motion for general sinusoidal flows we will now discuss the corresponding gravitational potentials. These are obtained by inserting Eq. (15) into Eq. (4), yielding

$$U(y) = (-\frac{1}{2}A^2e^{-2y} + Ae^{-y}\cos x - \phi_0) |_{x=Z^{-1}(y)}, \tag{22}$$

where x is determined by its value on the free surface $y=Z(x)$. The inverse function Z^{-1} always exists if $Z'(x) \neq 0$ in $0 < x < \pi$. The gravitational potentials (22) are time varying as well as spatially nonuniform. For special evolution laws of the amplitude one can, however, model conditions of general interest.

A particularly simple example is obtained by setting $\phi_0=0$ and $A=1$. Then Eq. (22) reduces to a time-independent potential of the form $U(y) = -e^{-2y}/2$. According to Eq. (17) the bubble and spike amplitudes grow as $y = \ln(1 \pm t)$, respectively. The bubble velocity is given by the square root of the local acceleration, $v_y = (\partial_y U)^{1/2}$, and the spike tip falls freely with velocity $v_y = -(-2U)^{1/2}$. As a result of the exponentially increasing acceleration it reaches infinity at the finite time $t=1$. Because of its inherent simplicity this solution may be used as a convenient test for general computational methods.

In terms of sinusoidal flow fields the closest approach to classical uniform acceleration is obtained by the requirement of constant acceleration g near the bubble vertex. This condition is most easily taken into account in the comoving frame where Eqs. (5) and (20) define the gravitational potential,

$$U(y+a) - U(a) = [\ddot{a}(e^{-y}\cos x - 1) + \frac{1}{2}\dot{a}^2(2e^{-y}\cos x - 1 - e^{-2y})] |_{x=Z^{-1}(y)}. \tag{23}$$

The amplitude $a(t)$ now is determined by the condition $U'(0)=1$ and $y = -cx^2/2$ near $y=0$. Expanding in Eqs. (2) and (23) about $x=y=0$ up to the order $O(x^2)$ one finds coupled equations governing the evolution of the bubble amplitude and curvature,

$$\ddot{a} + \frac{\dot{a}^2}{1-c} - \frac{c}{1-c} = 0, \quad \dot{c} = \dot{a}(1-3c). \tag{24}$$

Integration yields

$$c = (1-fh)/3, \tag{25}$$

$$\dot{a}^2 = \frac{\frac{2}{3}(1-h) - h[2f(a-a_0) - \dot{a}_0^2(2+f)]}{2+fh}$$

with $f=1-3c_0$, $h=e^{-3(a-a_0)}$, and where the index 0 denotes the initial value of the corresponding variable. For large amplitudes one has $h \ll 1$ and then Eq. (25) reduces to $c = \frac{1}{3}$ and $\dot{a} = 1/\sqrt{3}$. This limit describes the steady bubble (19) rising with a constant velocity. It is usual to express the bubble velocity in units of $\sqrt{g\lambda}$ as the Froude number F and the curvature κ by the dimensionless number $\kappa\lambda$. Then their steady values are given by $F = \dot{a}/\sqrt{2\pi} = 1/\sqrt{6\pi}$ and $\kappa\lambda = 2\pi c = 2\pi/3$.

Let us now discuss the validity of these results for uniform acceleration. The accuracy of the approximation there may be judged from a comparison of the gravitational potentials. For an initial perturbation $y = a_0(\cos x - 1)$, $\dot{a}_0 = 0$ the initial gravitational potential follows from Eqs. (23) and (24) to be

$$U(y+a_0) - U(a_0) = [(a_0+y)e^{-y} - a_0]/(1-a_0). \tag{26}$$

The steady-state gravitational potential is obtained from Eqs. (19) and (23) by setting $\ddot{a}=0$ and $\dot{a}^2 = \frac{1}{3}$. These po-

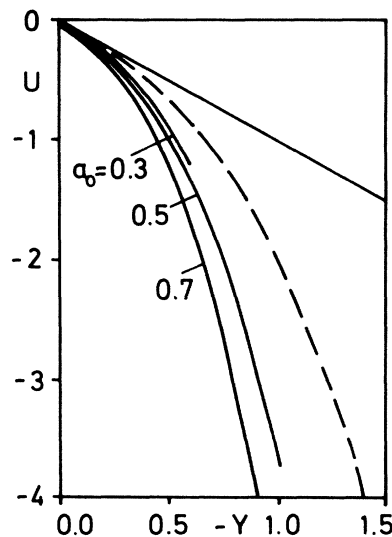


FIG. 8. Gravitational potentials for prescribed constant acceleration at the bubble maximum. The initial potentials as given by Eq. (26) are shown for different initial amplitudes a_0 and the steady-state potential is marked by a dashed line.

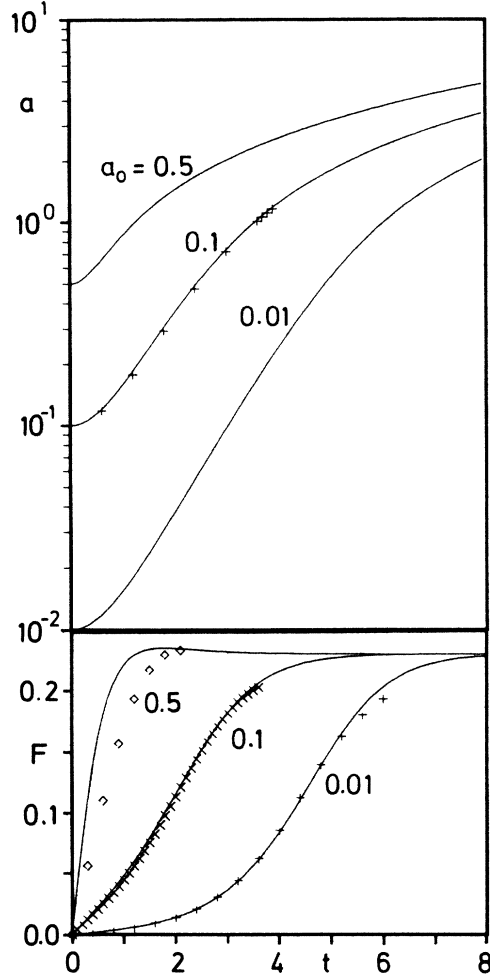


FIG. 9. Evolution of the bubble amplitude a and the Froude number $F = \dot{a}/\sqrt{2\pi}$ in Layzer's model. Comparison is made with the LSA calculations (marker symbols). The agreement is found best for small initial amplitudes where Fig. 8 shows smaller deviations in the initial gravitational accelerations.

tentials have been compared with their linear approximation at $y=0$ (Fig. 8). It can be seen that the actual gravitational acceleration here is rapidly increasing below the stagnation point and that this increase becomes worse for larger initial amplitudes. The time evolution of the bubble amplitude and the bubble velocity as given by Eq. (25) is shown in Fig. 9 for sinusoidal initial perturbations with $a_0=0.01, 0.1, 0.5$ and $\dot{a}_0=0$. Comparison is made with the numerical results for uniform acceleration as obtained by least-squares approximation (Sec. III). The agreement is found to be surprisingly good, indicating only weak dependence of the bubble velocity on the acceleration nonuniformities along the falling spike. The analytic model tends to slightly overestimate the velocities which may be expected from the increasing acceleration there. A more sensitive parameter, however, is the bubble curvature. The steady-state value is only about $\frac{2}{3}$ of the values obtained by computational methods. To account for this discrepancy an improved model of steady-state bubbles will be considered in the following section.

V. SOURCE FLOWS

To obtain a better approximation for uniform acceleration we now consider a larger class of steady flows which includes sinusoidal flow as a special case. Such a generalization proves possible in terms of a source model. To satisfy periodicity requirements such flows will consist in the simplest case of an infinite row of equally spaced isolated sources. A single plane source at the origin is described by a complex potential $W = \phi + i\psi$ of the form $W = c \text{Ln}z$ where $z = x + iy$ and c denotes the source strength. The potential of a row of sources of strength $c = 1$ at the points $x = 2\pi n$, $n = 0, \pm 1, \pm 2, \dots$, on the x axis then follows to be³⁸

$$\begin{aligned} W &= \sum_{n=-\infty}^{+\infty} \text{Ln}(z - 2\pi n) \\ &= \text{Ln} \left\{ \frac{z}{2} \prod_{n=1}^{\infty} \left[1 - \left(\frac{z/2}{n\pi} \right)^2 \right] \right\} + \text{const} \\ &= \text{Ln} \sin(z/2) + \text{const} . \end{aligned} \quad (27)$$

Separating real and imaginary parts Eq. (27) yields, up to a constant,

$$\phi = \frac{1}{2} \ln[\cosh(y) - \cos x] , \quad (28)$$

$$\psi = \arctan[\cot(x/2)\tanh(y/2)] .$$

In the bubble frame this source row has to be combined with a uniform stream perpendicular to the row. The resulting flow can be described in the form

$$\phi = [u/(2q)] \{ -(1+q)y + (1-q)\ln[\cosh(y) - \cos(x)] \} , \quad (29)$$

$$\psi = [u/(2q)] \{ (1+q)x + 2(1-q)\arctan[\cot(x/2)\tanh(y/2)] \} .$$

The parameter $u > 0$ denotes the velocity of the incoming stream at $y = +\infty$ where $\phi \rightarrow -uy$. At $y = -\infty$ one has $\phi \rightarrow -(u/q)y$ corresponding to an outgoing stream of velocity u/q . To imitate bubble flows the parameter q is restricted to the values $0 < q < 1$. The bubble surface is obtained by the streamline $\psi = u(1-q)\pi/(2q)$ through the stagnation point at $x=0$ yielding

$$y = \ln[\sin \bar{x} / \sin(q\bar{x})] , \quad (30)$$

with $\bar{x} = x/(1-q)$. Expanding about $x=0$ one finds the bubble maximum at $y = -\ln q$ and the curvature by

$$\kappa\lambda = \frac{2}{3} \frac{1+q}{1-q} \pi . \quad (31)$$

It is noted that the above result (19) here is recovered for $q \rightarrow 0$. In this limit the bubble maximum lies far above the source row where the velocity potential (29) approaches sinusoidal form. For finite q , however, one can model different bubble shapes which allow better agreement for uniform acceleration (Fig. 10).

The gravitational potentials are determined by Eqs. (5) and (30). They describe a potential difference

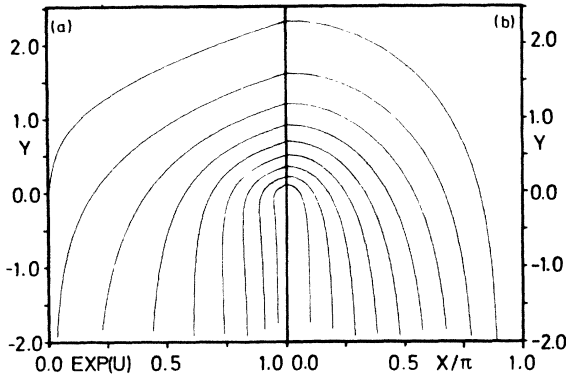


FIG. 10. (a) Gravitational potential and (b) corresponding bubble shapes in the source flow model. The source is located at the origin $x=y=0$ and the curves emanate from the stagnation point at $y=-\ln q$. The parameter q is varied in steps of 0.1 from 0.1 to 0.9.

$\Delta U = u^2/(2q^2)$ between the stagnation point and the asymptotic regime at $y = -\infty$. Imposing the normalization condition $U'(y)=1$ at the bubble maximum the Froude number is found to be

$$F = \left(\frac{1-q^2}{6\pi} \right)^{1/2}. \quad (32)$$

Comparing the gravitational potentials for different q with their linear approximation at the bubble maximum one finds the best approach to uniform acceleration for $q \sim 0.2$ (Fig. 11). In this case Eq. (31) yields the curvature $\kappa\lambda = \pi$ and Eq. (32) the Froude number $F \sim 0.226$. Both

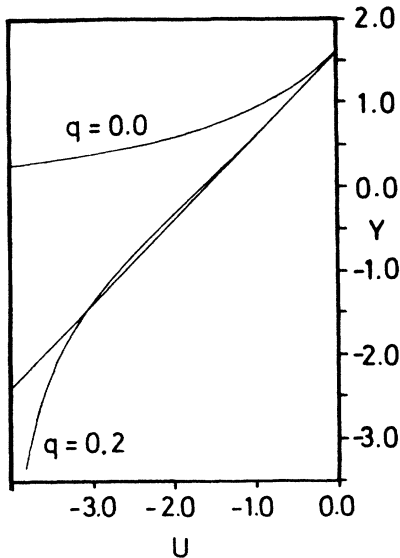


FIG. 11. Comparison of gravitational potentials for constant acceleration (straight line), steady sinusoidal flow ($q=0$), and source flow with $q=0.2$. At $y = -1.5$ where the potential for $q=0.2$ starts deviating from the linear potential the fluid is already close to free fall.

values are found in excellent agreement with recent computational results.³⁴ To discuss the amplitudes of the harmonics in this solution we derive the Fourier-series representation of the source potential (28) in the half-planes $|y| > 0$. It is convenient to start here with the series of

$$\partial_y \phi = \frac{v_0}{2} + \sum_{m=1}^{\infty} v_m \cos(mx), \quad (33)$$

where the coefficients are given by

$$v_m = \frac{1}{2\pi} \int_{-\pi}^{+\pi} dx \cos(mx) \frac{\sinh(y)}{\cosh(y) - \cos(x)}.$$

Introducing a complex integration variable with imaginary part x then yields

$$v_m = \frac{1}{2\pi i} \int_{-i\pi}^{+i\pi} ds e^{ms} \frac{\sinh(y)}{\cosh(y) - \cosh(s)}. \quad (34)$$

The integrand has poles at the points $s = s_p = \pm |y|$ on the real axis. In their neighborhood the denominator is represented by $\cosh(y) - \cosh(s) \sim -\sinh(s_p)(s - s_p)$. Choosing the integration contour connecting the points $-i\pi, +i\pi, -\infty + i\pi$, and $-\infty - i\pi$, one finds, by the residuum theorem,

$$v_m = e^{-m|y|} \frac{\sinh(y)}{-\sinh(-|y|)} = \text{sgn}(y) e^{-m|y|}, \quad (35)$$

where $\text{sgn}(y) = \pm 1$ for $y = \gtrless 0$, respectively. From Eqs. (33), (35), and the boundary condition $\phi(|y| \rightarrow \infty) = -\frac{1}{2} \ln 2 + |y|/2$ the Fourier series of the potential (28) is found to be

$$\phi = -\frac{\ln 2}{2} + \frac{|y|}{2} - \sum_{m=1}^{\infty} m^{-1} e^{-m|y|} \cos(mx). \quad (36)$$

Note that far from the sources where $|y| \gg 1$ the contribution of the harmonics decreases and the flow becomes approximately sinusoidal. At the bubble vertex where $y = -\ln q$ the Fourier coefficients are given by q^m/m .

VI. CONCLUSIONS

In this paper we analyzed the free-surface RT instability by the general method of LSA and by analytic models based on sinusoidal and source potentials. The LSA results have been found satisfactory for the initial and transient stages of the evolution, but the method fails in the final steady-state regime. This is a consequence of an only poor convergence of Fourier series, which will even fail to converge when flow singularities develop. Such failure can be expected for quite general reasons. Let us assume steady bubbles rising with velocity u and described by time-independent Fourier coefficients ϕ'_m in the comoving bubble frame. The Fourier coefficients in the laboratory frame then will be given by $\phi_m(t) = \phi'_m e^{mut}$ for $m \geq 1$. These correspond to modes having an initial spectrum ϕ'_m and dimensionless growth rates $\gamma_m = mu$. Note that these steady-state growth rates increase even faster with the mode number than the linear ones, $\gamma_m = \sqrt{m}$. Therefore, if the initial spectrum ϕ'_m includes an infinite number of modes, the Fourier series must fail to converge after a transition time of order $t \sim u^{-1}$. Fur-

ther improvement of the LSA method will possibly require the use of other sets of approximating functions. Better convergence properties may be expected for eigenfunction expansions. However, the calculation of eigenfunctions, corresponding to the instantaneous shape of the fluid, will greatly complicate the computational effort.

The sinusoidal flow model treats the evolution exactly for specific initial conditions and accelerations. Remarkably, the same asymptotic bubble shape can be found for substantially different types of acceleration. In the first example of Sec. IV the evolution starts from a large velocity perturbation and the acceleration at the bubble maximum decreases in time as $(1+t)^{-2}$. These conditions are qualitatively similar to impulsive acceleration as produced by shock waves.³⁹ In the second example of Sec. IV the interface is initially at rest and the bubble maximum is subject to constant acceleration. This corresponds closely to the classical instability problem and the bubble velocities there are found in close agreement with the LSA results. As a simple application of this model we will estimate the critical wave-number regime for foil breaking. We define foil breaking by the condition $a_1 = a_2 + d$, where a_1 denotes the displacement amplitude at the front, a_2 at the rear side of the foil, and d the unperturbed foil thickness. The amplitude a_2 is only appreciable for thin foils. There the foil breaks at small amplitudes, so that a_2 can be well approximated by linear theory as $a_2 = a_1 e^{-kd}$. The critical amplitude for a_1 , where foil breaking occurs, then is given by $a_c = d / (1 - e^{-kd})$. For thick foils it is determined by the foil thickness, $a_c = d$, and for thin foils by the wavelength, $ka_c = 1$. In Fig. 12 we compare the growth of perturbations with different wavelengths for given initial amplitudes, $ka_0 = 0.01$, as determined by Eq. (24). It can be seen that the maximum growth occurs for intermediate wavelengths of the order of the foil thickness. Large wavelengths are suppressed

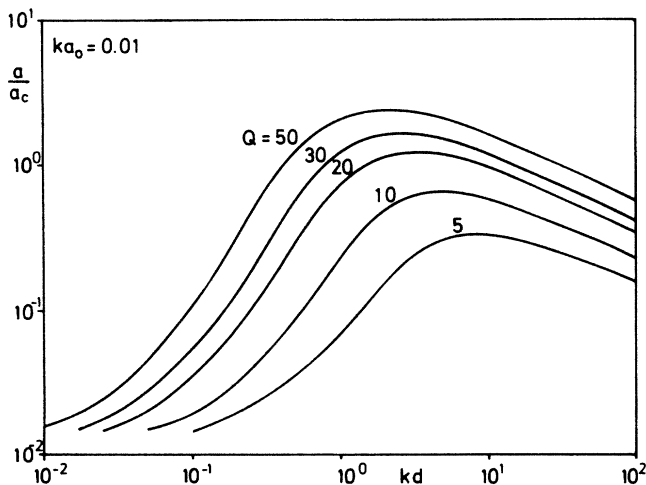


FIG. 12. Stability of an accelerated foil of thickness d under free-surface perturbations of amplitude a and wave number k . The foil is expected to break when the amplitudes have grown from the initial value a_0 to the critical value $a_c = d / (1 - e^{-kd})$. This occurs first for $kd \sim 2-3$ when $Q = \frac{1}{2}gt^2/d \sim 20$.

during the linear growth regime and small wavelengths during the final steady state. The time evolution can be described by the parameter $Q = \frac{1}{2}gt^2/d$, which is the ratio of the acceleration distance of the foil over the foil thickness. The critical amplitude here is reached first for the wave numbers $kd = 2-3$ when $Q \sim 20$.

The source model improves the estimates of the relevant bubble parameters. There the Froude number F and curvature κ are given by

$$F = \left[\frac{1-q^2}{6\pi} \right]^{1/2}, \quad \kappa\lambda = \frac{2}{3} \frac{1+q}{1-q} \pi. \quad (37)$$

The parameter q in the interval $0 \leq q < 1$ describes a family of possible bubbles when the fluid is falling through a potential difference $\Delta U = u^2 / (2q^2)$. The best approach to constant acceleration is found for $q = 0.2$ with $F = 0.226$ and $\kappa\lambda = \pi$.

ACKNOWLEDGMENTS

The author would like to thank P. Mulser, J. Meyerter-Vehn, R. Sigel, and S. Witkowski for valuable discussions and continuous encouragement. This study was supported by the Bundesministerium für Forschung und Technologie (Bonn, Germany).

APPENDIX A: TRANSFORMATION OF BERNOULLI'S EQUATION UNDER TIME-DEPENDENT TRANSLATIONS

We consider Eq. (5) under the coordinate transformation

$$x' = x, \quad y' = y - a(t), \quad (A1)$$

where $a(t)$ denotes the bubble amplitude. The transformation (A1) conserves vorticity and therefore potential flow in the frame F can also be described by a potential $\phi'(x', y', t)$ in F' . The corresponding transformations of the potentials and velocities are

$$\phi'(x', y', t) = \phi(x, y, t) - \dot{a}y' + \psi_0(t), \quad (A2)$$

$$v'_x = v_x, \quad v'_y = v_y - \dot{a},$$

where $\psi_0(t)$ allows for an arbitrary gauge of ϕ' . Considering $\phi(x, y, t) = \phi(x', y' + a, t)$ as a function of the primed arguments yields

$$\partial_t \phi|_y = \partial_t \phi|_{y'} - \partial_{y'} \phi|_t \dot{a}. \quad (A3)$$

Inserting now Eq. (A2) into Eq. (A3), one finds

$$\partial_t \phi|_y = \partial_t \phi'|_{y'} + \ddot{a}y' - \dot{\psi}_0 - \dot{a}(v'_y + \dot{a}). \quad (A4)$$

Using Eqs. (A1), (A2), and (A4) it is easily seen that Eq. (4) transforms into

$$\begin{aligned} \partial_t \phi'|_{y'} + \frac{1}{2}(v')^2 + U(a + Z') - U(a) + \ddot{a}Z' \\ = \frac{1}{2}\dot{a}^2 + \dot{\psi}_0 - U(a). \end{aligned} \quad (A5)$$

Choosing now the gauge, $\dot{\psi}_0 = U(a) - \frac{1}{2}\dot{a}^2$, one obtains Eq. (5). With this choice the velocity potential ϕ' is constant at the origin, where $v' = Z' = 0$.

APPENDIX B: DERIVATIVES
OF THE ORTHONORMAL FUNCTION SYSTEM $\{g_m\}$

To evaluate the function R of Eq. (7) one has to know the partial derivatives of the orthonormal function system $\{g_m\}$. The spatial derivatives $\partial_x g_m$ and $\partial_y g_m$ are readily obtained from the corresponding derivatives of h_m as defined under Eq. (12). The time derivative is somewhat more involved and therefore will be given here explicitly. From the definition $g_m = h_m / \|h_m\|$ one has

$$\partial_t g_m = \frac{\partial_t h_m}{\|h_m\|} - g_m \frac{\frac{d}{dt} \|h_m\|}{\|h_m\|}. \quad (\text{B1})$$

The derivative $\partial_t h_m$ can be calculated from

$$\partial_t h_m = - \sum_{i=0}^{m-1} \left((g_i, f_m) \partial_t g_i + g_i \frac{d}{dt} (g_i, f_m) \right), \quad (\text{B2})$$

where

$$\begin{aligned} \frac{d}{dt} (g_i, f_m) &= (\partial_t g_i + \dot{x} \partial_x g_i + \dot{y} \partial_y g_i, f_m) \\ &+ (g_i, \dot{x} \partial_x f_m + \dot{y} \partial_y f_m) \end{aligned}$$

and

$$\dot{x} = \sum_{m=0}^{r-1} c_m \partial_x g_m, \quad \dot{y} = \sum_{m=0}^{r-1} c_m \partial_y g_m.$$

The derivative $(d/dt)\|h_m\|$ then may be eliminated from the identity,

$$0 = \frac{d}{dt} \|g_m\|^2 = 2(g_m, \partial_t g_m + \dot{x} \partial_x g_m + \dot{y} \partial_y g_m), \quad (\text{B3})$$

yielding

$$\frac{\frac{d}{dt} \|h_m\|}{\|h_m\|} = (g_m, \partial_t h_m / \|h_m\| + \dot{x} \partial_x g_m + \dot{y} \partial_y g_m).$$

Equations (B2) and (B3) express the derivative (B1) by known quantities at a given time.

- ¹G. Taylor, Proc. R. Soc. London, Ser. A **201**, 192 (1950).
²J. N. Shiau, E. B. Goldman, and C. I. Weng, Phys. Rev. Lett. **32**, 352 (1974).
³S. E. Bodner, Phys. Rev. Lett. **33**, 761 (1974).
⁴D. R. Henderson, R. L. McCrory, and R. L. Morse, Phys. Rev. Lett. **33**, 205 (1974).
⁵K. A. Brueckner, S. Jorna, and R. Janda, Phys. Fluids **17**, 1554 (1974).
⁶J. D. Lindl and W. C. Mead, Phys. Rev. Lett. **34**, 1273 (1975).
⁷C. P. Verdon, R. L. McCrory, R. L. Morse, G. R. Baker, D. I. Meiron, and S. A. Orszag, Phys. Fluids **25**, 1653 (1982).
⁸M. H. Emery, J. H. Gardner, and J. P. Boris, Phys. Rev. Lett. **48**, 677 (1982).
⁹R. G. Evans, A. J. Bennett, and G. J. Pert, Phys. Rev. Lett. **49**, 1639 (1982).
¹⁰H. Takabe, L. Montierth, and R. L. Morse, Phys. Fluids **26**, 2299 (1983).
¹¹D. L. Hill and J. A. Wheeler, Phys. Rev. **89**, 1102 (1953).
¹²L. Spitzer, Astrophys. J. **120**, 1 (1954).
¹³M. H. Schneps, P. T. P. Ho, and A. H. Barrett, Astrophys. J. **240**, 84 (1980).
¹⁴J. R. Buchler, M. Livio, and S. A. Colgate, Space Sci. Rev. **27**, 571 (1980).
¹⁵L. Smarr, J. R. Wilson, R. T. Barton, and R. L. Bowers, Astrophys. J. **246**, 515 (1981).
¹⁶D. J. Lewis, Proc. R. Soc. London, Ser. A **202**, 81 (1950).
¹⁷H. W. Emmons, C. T. Chang, and B. C. Watson, Fluid Mech. **7**, 177 (1960).
¹⁸M. Ratafia, Phys. Fluids **16**, 1207 (1973).
¹⁹J. Grun and S. Kacenjar, Appl. Phys. Lett. **44**, 498 (1984).
²⁰M. A. Sweeney and F. C. Perry, J. Appl. Phys. **52**, 4487 (1981).
²¹B. Amini, Phys. Fluids **28**, 387 (1985).
²²R. M. Davies and G. Taylor, Proc. R. Soc. London, Ser. A **200**, 375 (1950).
²³D. Layzer, Astrophys. J. **122**, 1 (1955).
²⁴H. J. Kull, Phys. Rev. Lett. **51**, 1434 (1983).
²⁵H. J. Kull, Phys. Rev. A **31**, 540 (1985).
²⁶C. T. Chang, Phys. Fluids **2**, 656 (1959).
²⁷A. H. Nayfeh, J. Fluid Mech. **38**, 619 (1969).
²⁸R. L. Kiang, Phys. Fluids **12**, 1333 (1969).
²⁹N. R. Rajappa, Acta Mech. **10**, 193 (1970).
³⁰G. Birkhoff and D. Carter, J. Math. Mech. **6**, 769 (1957).
³¹P. R. Garabedian, Proc. R. Soc. London, Ser. A **241**, 423 (1957).
³²R. Menikoff and C. Zemach, J. Comput. Phys. **51**, 28 (1983).
³³J. M. Vanden-Broeck, Phys. Fluids **27**, 1090 (1984); **27**, 2604 (1984).
³⁴G. R. Baker, D. I. Meiron, and S. A. Orszag, Phys. Fluids **23**, 1485 (1980).
³⁵R. Pennington (unpublished).
³⁶L. M. Milne-Thomson, *Theoretical Hydrodynamics* (MacMillan, London, 1968).
³⁷F. John, *Partial Differential Equations* (Springer, New York, 1978).
³⁸*Handbook of Mathematical Functions*, edited by M. Abramowitz and I. A. Stegun (Dover, New York, 1972).
³⁹R. D. Richtmyer, Commun. Pure Appl. Math. **XII**, 297 (1960).